

# A Possible Subclassification of Fast Radio Bursts

Han-Yue Guo<sup>\*</sup> and Hao Wei<sup>†</sup>

*School of Physics, Beijing Institute of Technology, Beijing 100081, China*

## ABSTRACT

Although fast radio bursts (FRBs) have been an active field in astronomy and cosmology, their origin is still unknown to date. One of the interesting topics is the classification of FRBs, which is closely related to the origin of FRBs. Different physical mechanisms are required by different classes of FRBs. In the literature, they usually could be classified into non-repeating and repeating FRBs. Well motivated by the observations, here we are interested in the possible subclassification of FRBs. By using the first CHIME/FRB catalog, we propose to subclassify non-repeating (type I) FRBs into type Ia and Ib FRBs. The distribution of type Ia FRBs is delayed with respect to the cosmic star formation history (SFH), and hence they are probably associated with old stellar populations, while the distribution of type Ib FRBs tracks SFH, and hence they are probably associated with young stellar populations. Accordingly, the physical criteria for this subclassification of type I FRBs have been clearly determined. We find that there are some tight empirical correlations for type Ia FRBs but not for type Ib FRBs, and vice versa. These make them different in physical properties. Similarly, we suggest that repeating (type II) FRBs could also be subclassified into type IIa and IIb FRBs. A universal subclassification scheme is given at the end. This subclassification of FRBs might help us to reveal quite different physical mechanisms behind them, and improve their applications in astronomy and cosmology.

PACS numbers: 98.70.Dk, 98.70.-f, 97.10.Bt, 97.10.Ri, 95.30.Gv

---

<sup>\*</sup> email address: guohanyue7@163.com

<sup>†</sup> Corresponding author; email address: haowei@bit.edu.cn

## I. INTRODUCTION

Although fast radio bursts (FRBs) have been an active field in astronomy and cosmology, their origin is still unknown to date. FRBs are mysterious transient radio sources of millisecond duration [1–15]. Most of them are at extragalactic/cosmological distances, as suggested by their large dispersion measures (DMs) well in excess of the Galactic values, and hence FRBs are a promising probe to study cosmology and the intergalactic medium (see e.g. [51–58] and also [1–15]).

To reveal the possible origins of FRBs, various topics are extensively debated in the literature [1–15], such as the engine, radiation mechanism, distribution, classification, propagation effect, and cosmological application of FRBs. Many theoretical models have been proposed to this end, and we refer to e.g. [6–13] for comprehensive reviews and [16] for the up-to-date online catalogue of FRB theories. On the other hand, the observational data were rapidly accumulated in the recent years [10–14, 17, 18]. Therefore, many impressive progresses have been made in the field of FRBs.

One of the interesting topics is the classification of FRBs [4, 6–8, 10]. How many different populations of FRBs exist? In the actual observations, many FRBs were found to be (apparently) one-off, while some FRBs are repeating. So, it is natural to classify them into two populations: non-repeating FRBs and repeating FRBs. This classification is closely related to the origin of FRBs. Obviously, the repeaters rule out the cataclysmic engines for these sources. However, the question is whether the apparently non-repeating FRBs are genuinely one-off or not. In fact, some apparently non-repeating FRBs were found to be repeaters in the follow-up observations. It is possible that all FRBs repeat, and the non-detection of repetition might be due to the long waiting time or low flux of the repeating bursts (see e.g. [19–21]), or an unknown selection effect [22]. Some unified models for repeating and non-repeating FRBs were proposed in the literature (see e.g. [23–26]). Recently, some works have tried to address this question. In [20], the number fraction of repeating FRBs was predicted to peak at a value less than 100% in the future if non-repeating FRBs are genuinely one-off, otherwise it will increase to 100% eventually. In [27], it was found that the time-integrated-luminosity functions and volumetric occurrence rates of non-repeating and repeating FRBs against redshift are significantly different. In [28], it was claimed that the discriminant properties in FRBs is difficult to be explained by a single population. In [29], an observed difference in the burst morphologies of one-off FRBs and repeater bursts was found. The above works indicate that it is reasonable to classify them into repeating and non-repeating FRBs.

Another natural question is whether there are other classifications of FRBs different from repeating and non-repeating FRBs. Recently, several efforts were made in the literature. In [30], similar to gamma-ray bursts (GRBs), it was proposed to classify FRBs into short ( $< 100$  ms) and long ( $> 100$  ms) FRBs. A tight power-law correlation between fluence and peak flux density was found for them. Long FRBs are more energetic than short FRBs in the fluence versus extragalactic DM plane. In [31], it was argued that the brightness temperature  $T_B$  might be used to classify the repeating bursts into classical ( $T_B \geq 10^{33}$  K) and atypical ( $T_B < 10^{33}$  K) ones in the light of the well-known repeating FRB 20121102A. A tight power-law correlation between pulse width and fluence was found for classical bursts. In [32], using cross-correlation and clustering algorithms applied to one-dimensional intensity profiles of the bursts, two major classes of FRBs featuring different waveform morphologies and simultaneously different distributions of brightness temperature were identified. These efforts might shed new light on the nature of FRBs.

In the present work, we are interested in the possible subclassification of FRBs. There are two main motivations for doing this. The first one comes from the neighboring fields of supernovae and GRBs. As is well known, there are two major classes of supernovae: type I and II [33]. Then, type I supernovae are subclassified into type Ia, Ib and Ic, while type II supernovae are subclassified into type II-P, II-L, II<sub>n</sub> and II<sub>b</sub>. Only the well-known type Ia supernovae could be used as standard candles, which led to the great discovery of cosmic acceleration (and Nobel prize in physics 2011). This highlights the importance of the subclassification. On the other hand, GRBs are usually classified into long and short ones. However, the existence of temporally long events showing signatures of short GRBs led to introduce an alternative classification: type I (typically short and associated with old populations) and type II (typically long and associated with young populations) [34, 35]. Similarly, our second motivation is related to FRBs associated with young or old populations. For a long time, it was speculated that the FRB distribution tracks the cosmic star formation history (SFH) [1–15]. The landmark Galactic FRB 200428 associated with the young magnetar SGR 1935+2154 [36–39] confirmed that at least some (if not all) FRBs originate from young magnetars. So, it is reasonable to expect that the FRB distribution is closely correlated with

star-forming activities, as observed for the repeating FRB 121102 [40], FRB 180916.J0158+65 [41], FRB 20190520B [42], FRB 20181030A [43], and FRB 20201124A [44, 77]. But it was argued in [45] that FRB 20201124A is located at an inter-arm region of a barred-spiral galaxy, namely an environment not directly expected for young populations. On the other hand, the recently discovered repeating FRB 20200120E in a globular cluster of the nearby galaxy M81 [46–48] suggested that some FRBs are associated with old stellar populations. In [49], it was claimed that the bursts of the first CHIME/FRB catalog [50] as a whole do not track SFH. In [51], it was independently confirmed that the FRB distribution model tracking SFH can be rejected at high confidence, and a suppressed evolution (delay) with respect to SFH was found. Putting the above facts together, it is reasonable to speculate that some FRBs are associated with young populations and hence they track SFH, while the other FRBs are associated with old populations and hence they do not track SFH. So, a possible subclassification of FRBs is required.

This paper is organized as followings. In Sec. II, we briefly introduce the observational data of FRBs, namely the first CHIME/FRB catalog [50]. In Sec. III, we show that the distributions of non-repeating and repeating FRBs are significantly different. For convenience, we suggest calling them type I and II FRBs, respectively. Then, we propose to subclassify non-repeating (type I) FRBs into type Ia and Ib FRBs. The distribution of type Ia FRBs is delayed with respect to SFH, and hence they are probably associated with old stellar populations, while the distribution of type Ib FRBs tracks SFH, and hence they are probably associated with young stellar populations. Accordingly, the physical criteria for this subclassification have been clearly determined. In Sec. IV, we find that there are some tight empirical correlations for type Ia FRBs but not for type Ib FRBs, and vice versa. These empirical correlations make them different in physical properties. Clearly, type Ia and Ib FRBs require quite different physical mechanisms. In Sec. V, we turn to repeating (type II) FRBs. In Sec. VI, some brief concluding remarks and a universal subclassification scheme are given.

## II. THE OBSERVATIONAL DATA

As is well known, one of the key observational quantities of FRBs is the dispersion measure DM, namely the column density of the free electrons, due to the ionized medium (plasma) along the path. Clearly, the observed DM of FRB can be separated into [51–58]

$$DM_{\text{obs}} = DM_{\text{MW}} + DM_{\text{halo}} + DM_{\text{IGM}} + DM_{\text{host}}/(1+z), \quad (1)$$

where  $z$  is the redshift, and  $DM_{\text{MW}}$ ,  $DM_{\text{halo}}$ ,  $DM_{\text{IGM}}$ ,  $DM_{\text{host}}$  are the contributions from the Milky Way, the Milky Way halo, the intergalactic medium (IGM), the host galaxy (including interstellar medium of the host galaxy and the near-source plasma), respectively. For convenience, one could introduce the extragalactic DM [51–58], namely

$$DM_{\text{E}} = DM_{\text{obs}} - DM_{\text{MW}} - DM_{\text{halo}} = DM_{\text{IGM}} + DM_{\text{host}}/(1+z). \quad (2)$$

Here, we adopt  $DM_{\text{halo}} = 30 \text{ pc cm}^{-3}$  (see e.g. [59, 60]), and  $DM_{\text{host}} = 50 \text{ pc cm}^{-3}$  (see e.g. [61–63]). In fact, they are the ones used in the literature for our Milky Way at high Galactic latitude. We can obtain  $DM_{\text{MW}}$  by using NE2001 [64–66] up to 30 kpc.  $DM_{\text{IGM}}$  is given by [51–58]

$$DM_{\text{IGM}} = \frac{3cH_0\Omega_b}{8\pi Gm_p} \int_0^z \frac{f_{\text{IGM}}(\tilde{z}) f_e(\tilde{z}) (1+\tilde{z}) d\tilde{z}}{h(\tilde{z})}, \quad (3)$$

where  $c$  is the speed of light,  $H_0$  is the Hubble constant,  $\Omega_b$  is the present fractional density of baryons,  $G$  is the gravitational constant,  $m_p$  is the mass of proton,  $h(z) \equiv H(z)/H_0$  is the dimensionless Hubble parameter,  $f_{\text{IGM}}(z)$  is the fraction of baryon mass in IGM, and  $f_e(z)$  is the ionized electron number fraction per baryon. The latter two are functions of redshift  $z$  in principle. Following e.g. [27, 49, 51, 55], we use the fiducial values  $f_e = 7/8$  and  $f_{\text{IGM}} = 0.82$  in this work. Note that it is very safe to adopt  $f_e = (3/4)\chi_{e,\text{H}}(z) + (1/4)\chi_{e,\text{He}}(z) = 7/8$  for  $\chi_{e,\text{H}}(z) = \chi_{e,\text{He}}(z) = 1$ , since hydrogen and helium are both fully ionized at  $z \leq 3$  for almost all observed FRBs [51–58]. Actually, the variation of  $f_{\text{IGM}}(z)$  is fairly small as it could be constrained by using other cosmological observations such as cosmic microwave background (see e.g. [52]), and hence it is also reasonable to adopt a constant  $f_{\text{IGM}}$  at low redshifts  $z \leq 3$ .

On the other hand, we consider the fiducial cosmology in this work, namely the well-known flat  $\Lambda$ CDM model, and hence

$$h(z) = \left[ \Omega_m (1+z)^3 + (1 - \Omega_m) \right]^{1/2}, \quad d_L = (1+z) d_C = c(1+z) \int_0^z \frac{d\tilde{z}}{H(\tilde{z})}, \quad (4)$$

where  $d_L$  and  $d_C$  are the luminosity distance and the comoving distance, respectively. In this work, we adopt  $\Omega_m = 0.3153$ ,  $\Omega_b = 0.0493$ , and  $H_0 = 67.36$  km/s/Mpc from the Planck 2018 results [67].

The first CHIME/FRB catalog [50] of 536 events (including 474 one-off bursts and 62 repeat bursts from 18 repeaters) was released in June 2021. Such a large uniform sample detected by a single telescope is very valuable to study FRBs. We preliminarily deal with it following [51]. At first, we exclude the bursts with zero fluences and the bursts labeled with `excluded_flag = 1`. Following e.g. [49, 51], we only use the first detected burst of each FRB source. In practice, we identify the non-repeaters labeled with `repeater_name = -9999` and then only take the ones labeled with `sub_num = 0` (434 bursts in total). We identify the repeaters labeled with `repeater_name  $\neq$  -9999` and only take the ones labeled with `sub_num = 0`, and then from them we adopt the first ones in each group with the same `repeater_name` (18 bursts in total). For each burst, its ‘‘observed’’  $DM_E = DM_{\text{obs}} - DM_{\text{MW}} - DM_{\text{halo}}$ , where  $DM_{\text{obs}}$  is given by the column labeled with ‘‘bonsai\_dm’’ in the data table. Then, its inferred redshift  $z$  is obtained by numerically solving  $DM_E = DM_{\text{IGM}} + DM_{\text{host}}/(1+z)$  with  $DM_{\text{IGM}}$  given by Eq. (3). In this work, we require a very conservative criterion  $DM_{\text{IGM}} \geq DM_{\text{obs}}/10$  to exclude the bursts very close to us. After this robust cut, we have 430 one-off FRBs and 17 repeaters.

For each burst, its observed specific fluence  $F_\nu$  is given by the column labeled with ‘‘fluence’’ in the data table. Assuming a flat radio spectrum, the specific fluence is related with isotropic energy  $E$  according to [49, 51, 68, 69]

$$F_\nu = \frac{(1+z)E}{4\pi d_L^2 \nu_c}, \quad (5)$$

where  $\nu_c$  is the central observing frequency. For CHIME,  $\nu_c = 600$  MHz [50]. Thus, the ‘‘observed’’ isotropic energy  $E$  can be inferred from Eq. (5) with the observed  $F_\nu$  and the luminosity distance  $d_L$  given by Eq. (4). So far, the observational data of 430 one-off FRBs and 17 repeaters are ready.

### III. SUBCLASSIFICATION OF NON-REPEATING FRBS

#### A. Type I and II FRBs

In the radio sky, there are many known transients besides FRBs, such as pulsars, solar bursts, rotating radio transients (RRATs), nano-shots, flare stars/brown dwarves, X-ray binaries, RSCVn/Algols, novae, supernovae, AGN/blazar/QSO, giant radio pulses (GRPs), and GRBs. We refer to e.g. Fig. 1 of [3] for details. As is well known, they could be well distinguished in the transient duration  $\nu W$  versus spectral luminosity  $L_\nu$  phase plane, with the help of brightness temperature  $T_B$  which relates to the radiation mechanism (see e.g. Fig. 1 of [3], Fig. 5 of [70], Fig. 3 of [48], Fig. 7 of [7], and Fig. 4 of [71]).

Since the  $\nu W - L_\nu$  phase plane is very useful to distinguish radio transients, we might also use it to subclassify FRBs. In Fig. 1, we plot 430 one-off FRBs and 17 repeaters from the CHIME/FRB catalog in the  $\nu W - L_\nu$  plane, with some isothermal lines of  $T_B$ . For each burst, we take the frequency  $\nu$  and the pulse width  $W$  from the columns labeled with ‘‘peak\_freq’’ and ‘‘bc\_width’’ in the CHIME/FRB data table, respectively. We calculate the spectral luminosity  $L_\nu$  according to (e.g. [70, 71])

$$L_\nu = 4\pi d_L^2 S_\nu, \quad (6)$$

where the luminosity distance  $d_L$  is given by Eq. (4), and the flux  $S_\nu$  is given by the column labeled with ‘‘flux’’ in the CHIME/FRB data table. The brightness temperature  $T_B$  is given by (e.g. [31, 70, 71])

$$T_B = \frac{S_\nu d_L^2}{2\pi\kappa_B (\nu W)^2} = 1.1 \times 10^{35} \text{ K} \left( \frac{S_\nu}{\text{Jy}} \right) \left( \frac{d_L}{\text{Gpc}} \right)^2 \left( \frac{\nu}{\text{GHz}} \right)^{-2} \left( \frac{W}{\text{ms}} \right)^{-2}, \quad (7)$$

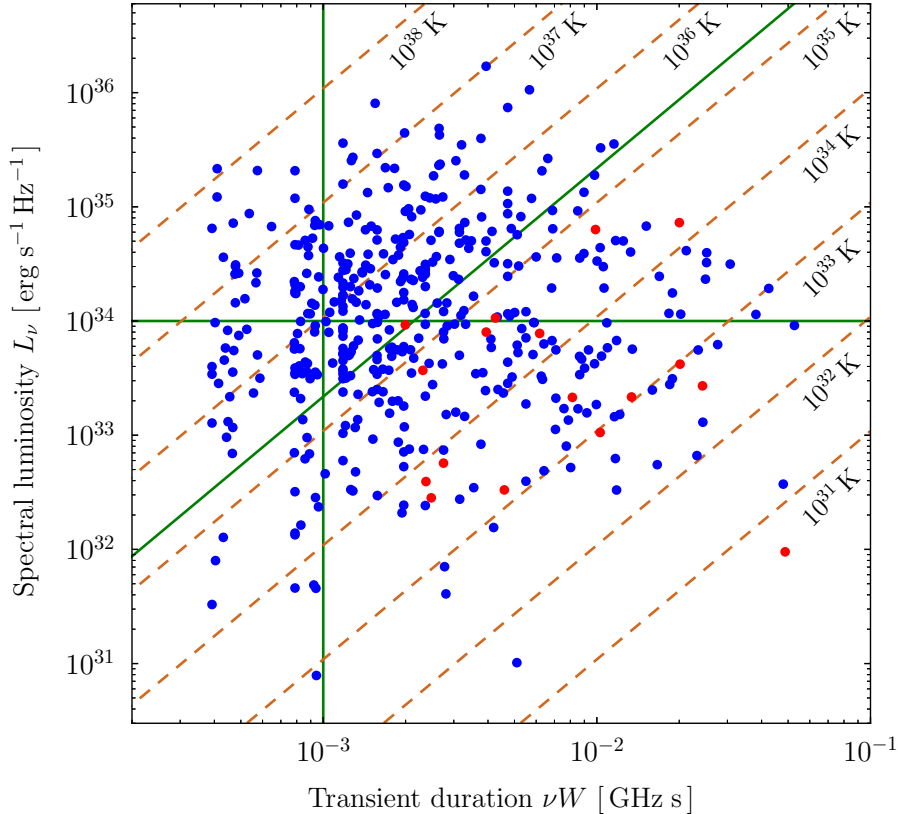


FIG. 1: 430 one-off FRBs (blue points) and 17 repeaters (red points) from the first CHIME/FRB catalog in the transient duration  $\nu W$  versus spectral luminosity  $L_\nu$  plane, with some isothermal lines of brightness temperature  $T_B$  (chocolate dashed lines). The green solid lines  $\nu W = 10^{-3}$  GHz s,  $L_\nu = 10^{34}$  erg/s/Hz and  $T_B = 2 \times 10^{35}$  K are used to divide this  $\nu W - L_\nu$  phase plane into various regions. See Sec. III and Fig. 3 for details.

which can be expressed in terms of  $\nu W$  and  $L_\nu$ .  $\kappa_B$  is the Boltzmann constant. It is worth noting that the above quantities might be slightly different in the literature (for example, in some works, the angular diameter distance  $d_A$  might be used instead of  $d_L$ , the central frequency  $\nu_c$  might be used instead of the peak frequency,  $\pi$  might be removed, the redshift might be introduced, and so on). We intentionally use them as the ones mentioned above, because they work well for our purpose in the present forms.

From Fig. 1, it is easy to see that the distributions of non-repeating and repeating FRBs are different in the  $\nu W - L_\nu$  phase plane. Clearly, most of the repeaters are located in the bottom-right region, where the transient duration  $\nu W$  is relatively large, the spectral luminosity  $L_\nu$  is relatively low, and the brightness temperature  $T_B$  is also relatively low. In Fig. 2, we present the normalized  $\nu W$ ,  $L_\nu$  and  $T_B$  distributions of non-repeating and repeating FRBs, respectively. Again, we find that these distributions are clearly different for non-repeaters and repeaters (note that the number of repeaters is only 17, and hence they do not form a good enough statistics). Thus, it is reasonable to classify FRBs into two types as usual. For convenience, we suggest calling non-repeating/repeating FRBs type I/II FRBs, respectively.

## B. Type Ia and Ib FRBs

At first, we consider the possible subclassification of non-repeating (type I) FRBs. By definition, the subclasses should be significantly different. As is well known, the Kolmogorov-Smirnov (KS) test is one of the useful tools to compare two samples [72]. One can perform the KS test by using `scipy.stats.kstest` in Python [73], which returns the KS statistic and the corresponding p-value. For convenience, we use the p-value ( $p_{\text{KS}}$ ) in the two-sample case as in [50, 51, 74], rather than the KS statistic ( $D_{\text{KS}}$ ). The null hypothesis (namely two samples are drawn from the same distribution) can be rejected at 90% (95%) confidence if  $p_{\text{KS}} < 0.1$  (0.05), respectively. Otherwise, two samples can be consistent with each other if

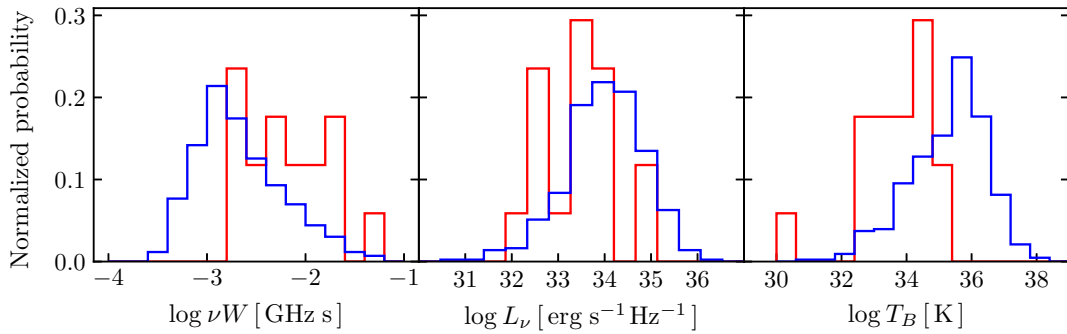


FIG. 2: Normalized  $\nu W$ ,  $L_\nu$  and  $T_B$  distributions of 430 non-repeaters (blue histograms) and 17 repeaters (red histograms), respectively. See Sec. III A for details.

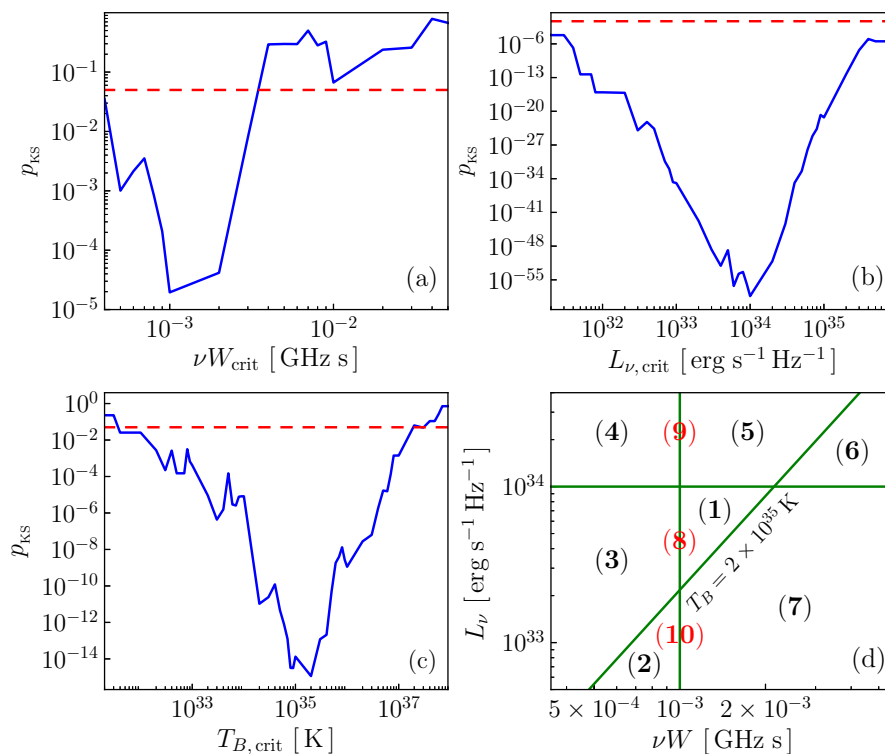


FIG. 3: The p-values  $p_{KS}$  are shown as functions of  $\nu W_{crit}$  (a),  $L_{\nu, crit}$  (b) and  $T_{B, crit}$  (c).  $p_{KS} = 0.05$  is indicated by the red dashed lines. In panel (d), the  $\nu W - L_\nu$  phase plane is divided into seven regions by the green solid lines  $\nu W = 10^{-3}$  GHz s,  $L_\nu = 10^{34}$  erg/s/Hz and  $T_B = 2 \times 10^{35}$  K. These 7 regions are labeled with the numbers (1)  $\sim$  (7). In addition, region (8) = regions (1) + (3), region (9) = regions (4) + (5), region (10) = regions (2) + (7). Panel (d) should be viewed together with Fig. 1. See Sec. III B for details.

$p_{KS} > 0.1$  (or 0.05).  $p_{KS}$  is higher for two closer samples (and  $p_{KS} = 1$  for two identical samples), while  $p_{KS} \rightarrow 0$  for two completely different samples.

There are three candidates ( $\nu W$ ,  $L_\nu$  and  $T_B$ ) in the  $\nu W - L_\nu$  phase plane for the possible criteria of subclassification. For a given critical value (say,  $\nu W_{crit}$ ), 430 non-repeating FRBs can be divided into two samples (say,  $\nu W \geq \nu W_{crit}$  and  $\nu W < \nu W_{crit}$ ), and then we compare the redshift distributions of these two samples by using the KS test. So, the p-values  $p_{KS}$  can be found as functions of  $\nu W_{crit}$ ,  $L_{\nu, crit}$  and  $T_{B, crit}$  by scanning their parameter spaces, respectively. We show them in Fig. 3. Note that two samples having a lower  $p_{KS}$  are more different. Thus, the minimal p-values indicate the best dividing lines. From panels (a), (b), (c) of Fig. 3, we find that the best dividing lines are given by  $\nu W = 10^{-3}$  GHz s,

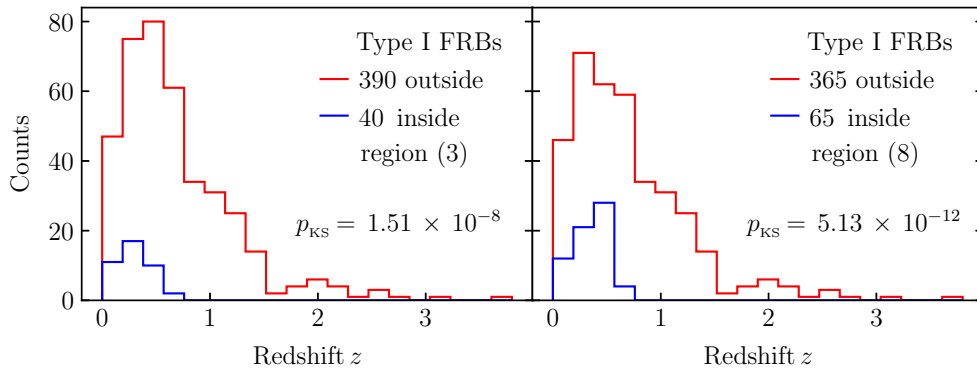


FIG. 4: Left panel: The redshift distributions of type I FRBs inside (blue) and outside (red) region (3). The numbers of these two samples are given, respectively. We also present the p-value  $p_{\text{KS}}$  of the KS test for these two redshift distributions. Right panel: The same as in left panel, but for region (8). See Sec. IIIB for details.

$L_\nu = 10^{34}$  erg/s/Hz and  $T_B = 2 \times 10^{35}$  K. They are plotted as the green solid lines in Fig. 1 and panel (d) of Fig. 3. Clearly, they divide the  $\nu W - L_\nu$  phase plane into seven regions, as labeled by the numbers (1)  $\sim$  (7) in panel (d) of Fig. 3.

As mentioned above, we speculate that some FRBs track SFH and the others do not. Their distributions should be significantly different. So far, we have divided the  $\nu W - L_\nu$  phase plane into 7 regions as above. For a given region, 430 non-repeating (type I) FRBs inside/outside this region form two samples. One can compare them by using the KS test. But now it is more important to see whether one of these two samples tracks SFH. Fortunately, a suitable method for this purpose was proposed in [49] and then has been extended in [51]. Here, we closely follow the method used in [51]. The key idea is to confront the Monte Carlo simulations with the observational data. If the simulations are rejected by the observational data, the assumed FRB distribution models generating these simulations could be ruled out. Otherwise, they survive. In the present work, we generate the simulations assuming SFH, namely the mock observed FRB redshift rate distribution is given by [49, 51]

$$\frac{dN}{dt_{\text{obs}} dz} = \frac{1}{1+z} \cdot \frac{dN}{dt dV} \cdot \frac{dV}{dz} = \frac{1}{1+z} \cdot \frac{dN}{dt dV} \cdot \frac{c}{H_0} \cdot \frac{4\pi d_C^2}{h(z)}, \quad (8)$$

where we have used  $dt/dt_{\text{obs}} = (1+z)^{-1}$  due to the cosmic expansion,  $d_C = d_L/(1+z)$  and  $h(z)$  are given by Eq. (4), and we assume that the distribution of mock FRBs track SFH [51, 75], namely

$$\frac{dN}{dt dV} \propto \text{SFH}(z) \propto \frac{(1+z)^{2.6}}{1 + ((1+z)/3.2)^{6.2}}. \quad (9)$$

Note that Eq. (9) is the best-fit SFH density from the latest observational data of ultraviolet and infrared surveys (see Eq. (1) of [75]), which characterizes the real SFH of our universe. On the other hand, we generate the isotropic energy  $E$  for the mock FRBs with [49, 51]

$$dN/dE \propto (E/E_c)^{-\alpha} \exp(-E/E_c), \quad (10)$$

where  $\alpha = 1.9$  and  $\log(E_c/\text{erg}) = 41$  are fixed as in [51], while “log” gives the logarithm to base 10. Notice that Eq. (10) corresponds to the Schechter luminosity function of FRBs [79, 80]. Actually, the isotropic energy distribution in Eq. (10) is characterized by a simple power law  $\propto E^{-\alpha}$  with a sharp exponential cutoff around the energy scale  $E_c$ . In the literature,  $\alpha$  and  $E_c$  could be constrained by the observations, i.e.  $1.8 \lesssim \alpha \lesssim 2$  roughly [69, 79, 81, 82] and  $E_c \sim 3 \times 10^{41}$  erg loosely [69, 79]. So,  $\alpha = 1.9$  and  $\log(E_c/\text{erg}) = 41$  are well consistent with the observations. One can generate  $N_{\text{sim}}$  mock FRBs tracking SFH as follows: (i) randomly assign a mock redshift  $z_i$  to the  $i$ -th mock FRB from the redshift distribution in Eq. (8) with Eq. (9); (ii) generate a mock energy  $E_i$  randomly from the distribution in Eq. (10) for this mock FRB; (iii) derive the specific fluence  $F_{\nu, i}$  by using Eq. (5) with  $z_i$  and  $E_i$  for this mock FRB; (iv) derive  $\text{DM}_{E, i}$  at redshift  $z_i$  by using Eq. (2) with Eq. (3) for this mock FRB; (v) repeat the above steps for  $N_{\text{sim}}$  times. Finally,  $N_{\text{sim}}$  mock FRBs are on hand.

$\log F_{\nu, \text{th}}^{\text{max}}$	$p_{\text{KS}}$ for $\log F_{\nu}$	$p_{\text{KS}}$ for $\log E$	$p_{\text{KS}}$ for $\text{DM}_{\text{E}}$
<b>0.77</b>	<b>0.2750</b>	<b>0.2859</b>	<b>0.4575</b>
0.78	0.3234	0.2530	0.3963
0.76	0.2266	0.2653	0.3944
0.84	0.8382	0.1714	0.6506

TABLE I: Some examples of the acceptable SFH models with the sensitivity model parameter  $\log F_{\nu, \text{th}}^{\text{max}}$ , and three  $p_{\text{KS}}$  for the  $\log F_{\nu}$ ,  $\log E$  and  $\text{DM}_{\text{E}}$  criteria against the CHIME/FRB data for 390 type I FRBs outside regions (3). The boldfaced ones are also presented in the accompanying plots. See Sec. III B for details.

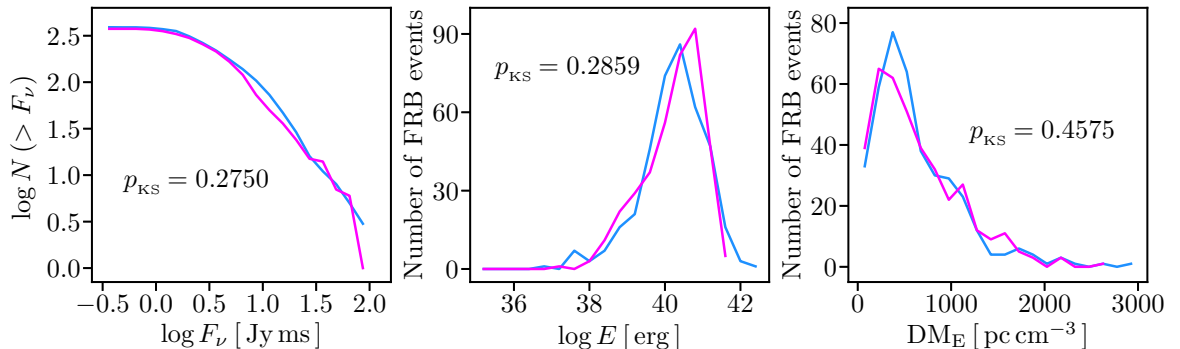


FIG. 5: The simulated SFH model with  $\log F_{\nu, \text{th}}^{\text{max}} = 0.77$  (magenta lines) against the CHIME/FRB data for 390 type I FRBs outside regions (3) (dodgerblue lines), with respect to the  $\log F_{\nu}$ ,  $\log E$  and  $\text{DM}_{\text{E}}$  criteria. Note that the simulations are all scaled to the CHIME/FRB data. The p-values  $p_{\text{KS}}$  of the KS tests are given, respectively. See Sec. III B for details.

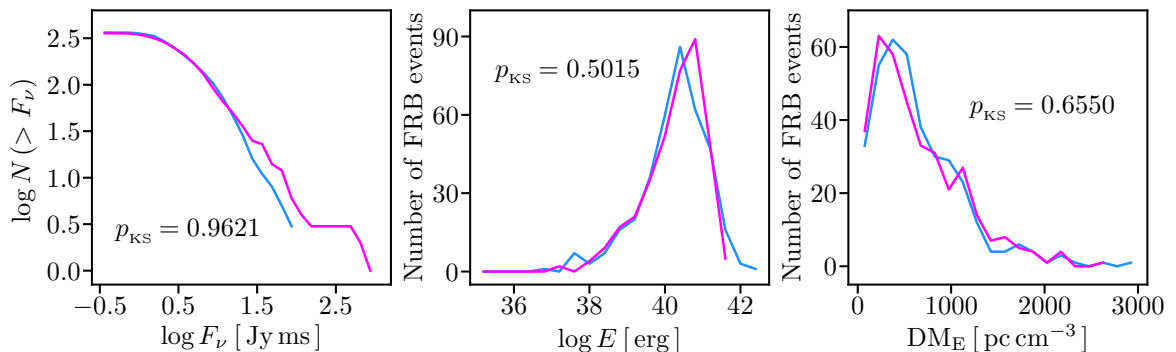
However, these  $N_{\text{sim}}$  mock FRBs intrinsically generated above are not the ones “detected” by the telescope, due to the telescope’s sensitivity threshold and instrumental selection effects near the threshold. Therefore, the next step is to filter them by using the telescope’s sensitivity model, which is difficult to characterize in fact. Here, we consider the simplified sensitivity model for CHIME following [49, 51], in which the sensitivity threshold is about 0.3 Jy ms for CHIME, or equivalently  $\log F_{\nu, \text{min}} = -0.5$ , where the specific fluence is in units of Jy ms. Due to the direction-dependent sensitivity of the telescope, there is a “gray zone” in the  $\log F_{\nu}$  distribution, within which CHIME has not reached full sensitivity to all sources [49, 51]. The detection efficiency parameter in the “gray zone” is given by  $\eta_{\text{det}} = \mathcal{R}^3$ , where  $\mathcal{R} = (\log F_{\nu, \text{th}} - \log F_{\nu, \text{th}}^{\text{min}}) / (\log F_{\nu, \text{th}}^{\text{max}} - \log F_{\nu, \text{th}}^{\text{min}})$ , such that  $\eta_{\text{det}} \rightarrow 0$  at  $\log F_{\nu, \text{th}}^{\text{min}} = -0.5$  and  $\eta_{\text{det}} \rightarrow 1$  at  $\log F_{\nu, \text{th}}^{\text{max}}$ . Outside the “gray zone”,  $\eta_{\text{det}} = 1$ . The filtered mock sample of FRBs will be confronted with the observational data, by using the KS tests with respect to the  $\log F_{\nu}$ ,  $\log E$  and  $\text{DM}_{\text{E}}$  distributions. In our case of SFH, the only free parameter is  $\log F_{\nu, \text{th}}^{\text{max}}$ , which should be adjusted to match the observation. Notice that there are a few minor differences between the present work and [51]. Here, we use slightly different  $\text{DM}_{\text{host}}$  and  $f_{\text{IGM}}$ , while we have required the very conservative cut  $\text{DM}_{\text{IGM}} \geq \text{DM}_{\text{obs}}/10$  to exclude the actual bursts very close to us in the first CHIME/FRB data table, as in Sec. II. In practice, most of these  $N_{\text{sim}}$  mock FRBs cannot pass the filter of sensitivity threshold and instrumental selection effects. To ensure that there are still enough mock FRBs ( $\sim \mathcal{O}(10^2)$ ), comparable with the number of observed FRBs) after the filter of sensitivity threshold and instrumental selection effects, we generate  $N_{\text{sim}} = 4,000,000$  mock FRBs in the simulation for our case of SFH. We strongly refer to [51] for the technical details.

Now, we test regions (1)  $\sim$  (7) in the  $\nu W - L_{\nu}$  phase plane one by one. For each region, 430 type I FRBs are divided into two samples inside or outside this region. We compare their redshift distributions by using KS test, and also check whether one of these two sample tracks SFH by using the above method closely following [51]. For 6 of these 7 regions, although their redshift distributions are fairly different, both samples of type I FRBs inside/outside the given region do not track SFH. The only survivor is



$\log F_{\nu, \text{th}}^{\text{max}}$	$p_{\text{KS}}$ for $\log F_{\nu}$	$p_{\text{KS}}$ for $\log E$	$p_{\text{KS}}$ for $\text{DM}_{\text{E}}$
<b>0.91</b>	<b>0.9621</b>	<b>0.5015</b>	<b>0.6550</b>
0.96	0.7832	0.5050	0.5656
0.94	0.8742	0.4341	0.7663
0.87	0.7526	0.4238	0.7071

TABLE II: The same as in Table I, but for 365 type I FRBs outside regions (8).

FIG. 6: The same as in Fig. 5, but for  $\log F_{\nu, \text{th}}^{\text{max}} = 0.91$  and 365 type I FRBs outside regions (8).

region (3), which is not so bad in some sense. It is defined by three physical conditions simultaneously

$$\text{Region (3)} : \nu W \leq 10^{-3} \text{ GHz s} \quad \& \quad L_{\nu} \leq 10^{34} \text{ erg/s/Hz} \quad \& \quad T_B \geq 2 \times 10^{35} \text{ K}. \quad (11)$$

As shown in left panel of Fig. 4, there are 40 (390) type I FRBs inside (outside) region (3), and their redshift distributions are significantly different, with a p-value  $p_{\text{KS}} = 1.51 \times 10^{-8} \ll 0.05$ . We find that the 40 type I FRBs inside region (3) do not track SFH. However, the 390 type I FRBs outside region (3) can be consistent with SFH. In Table I, we show some examples of the acceptable SFH models with the sensitivity model parameter  $\log F_{\nu, \text{th}}^{\text{max}}$ , and three  $p_{\text{KS}}$  for the  $\log F_{\nu}$ ,  $\log E$  and  $\text{DM}_{\text{E}}$  criteria against the CHIME/FRB data for 390 type I FRBs outside regions (3). For some suitable  $\log F_{\nu, \text{th}}^{\text{max}}$ , three p-values  $p_{\text{KS}} > 0.25$  simultaneously. We present an explicit example with  $\log F_{\nu, \text{th}}^{\text{max}} = 0.77$  in Fig. 5, whose three p-values  $p_{\text{KS}} > 0.27$  simultaneously. So, SFH cannot be rejected at high confidence by the CHIME/FRB data for 390 type I FRBs outside regions (3), although three p-values are not fairly high.

Could we improve these results? The answer is a loud yes. Let us come back to Fig. 3. From its panels (a), (b) and (c), we easily find that the p-value for the dividing line with respect to  $\nu W$  ( $\sim 2 \times 10^{-5}$ ) is much larger than the ones with respect to  $L_{\nu}$  ( $\sim 4 \times 10^{-59}$ ) and  $T_B$  ( $\sim 10^{-15}$ ). Thus, it is reasonable to discard the dividing line  $\nu W = 10^{-3} \text{ GHz s}$  from the  $\nu W - L_{\nu}$  phase plane to improve the situation. In this case, the  $\nu W - L_{\nu}$  phase plane is divided into 4 regions as shown in panel (d) of Fig. 3, namely region (8) = regions (1)+(3), region (9) = regions (4)+(5), region (10) = regions (2)+(7), and region (6). Again, we test these 4 regions one by one. We find that the last three regions fail. However, region (8) is very successful, which is defined by two physical conditions simultaneously

$$\text{Region (8)} : L_{\nu} \leq 10^{34} \text{ erg/s/Hz} \quad \& \quad T_B \geq 2 \times 10^{35} \text{ K}. \quad (12)$$

As shown in right panel of Fig. 4, there are 65 (365) type I FRBs inside (outside) region (8), and their redshift distributions are significantly different, with a p-value  $p_{\text{KS}} = 5.13 \times 10^{-12} \ll 0.05$  (note that this  $p_{\text{KS}}$  is also much smaller than the one for region (3), namely  $1.51 \times 10^{-8}$ ). We find that the 65 type I FRBs inside region (8) do not track SFH. But the 365 type I FRBs outside region (8) do track SFH at high confidence. In Table II, we show some examples of the acceptable SFH models with the

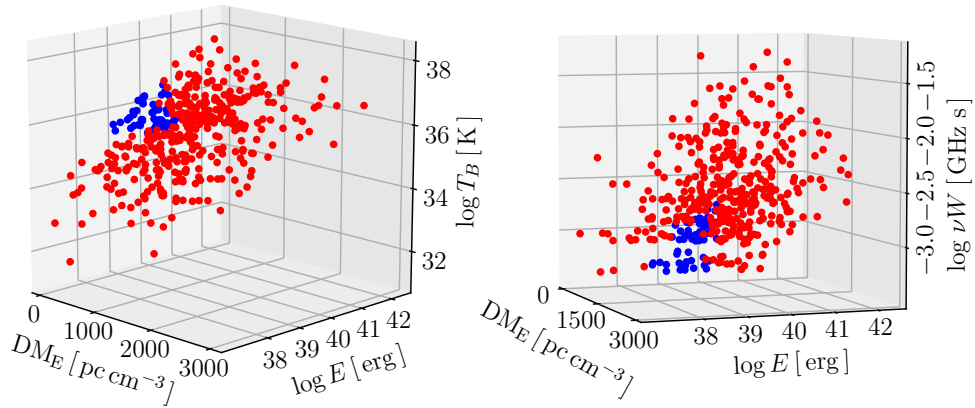


FIG. 7: Type Ia FRBs (blue points) and type Ib FRBs (red points) are located in distinct regions of 3-D spaces  $DM_E - \log E - \log T_B$  (left panel) or  $DM_E - \log E - \log \nu W$  (right panel). See Sec. IV for details.

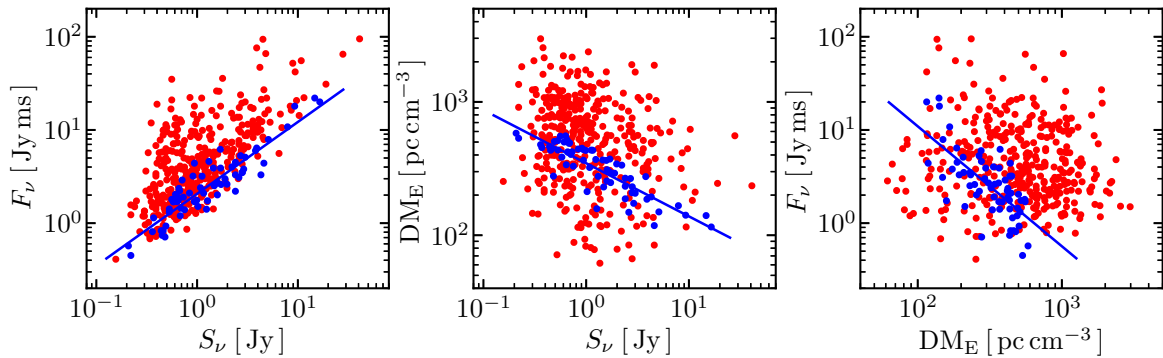


FIG. 8: The empirical correlations (blue lines) between fluence  $F_\nu$ , flux  $S_\nu$  and  $DM_E$  for 65 type Ia FRBs (blue points), but no such correlations for 365 type Ib FRBs (red points). See Sec. IV for details.

sensitivity model parameter  $\log F_{\nu, \text{th}}^{\text{max}}$ , and three  $p_{\text{KS}}$  for the  $\log F_\nu$ ,  $\log E$  and  $DM_E$  criteria against the CHIME/FRB data for 365 type I FRBs outside regions (8). Clearly, for some suitable  $\log F_{\nu, \text{th}}^{\text{max}}$ , three  $p$ -values  $p_{\text{KS}} > 0.5$  simultaneously. We present an explicit example with  $\log F_{\nu, \text{th}}^{\text{max}} = 0.91$  in Fig. 6. Thus, SFH can be fully consistent with the CHIME/FRB data for 365 type I FRBs outside regions (8).

So far, we have identified a special region (8) in the  $\nu W - L_\nu$  phase plane, which is defined by two physical conditions in Eq. (12) simultaneously. 430 type I FRBs are divided into two distinct samples. The 65 type I FRBs inside region (8) do not track SFH, and hence they are probably associated with old stellar populations. We suggest calling them type Ia FRBs. On the other hand, the 365 type I FRBs outside region (8) do track SFH, and hence they are probably associated with young stellar populations. We suggest calling them type Ib FRBs. In this way, we have achieved a physical subclassification of type I FRBs. From right panel of Fig. 4, it is easy to see that type Ib FRBs can appear at very high redshifts up to  $z \sim 3.7$ , but type Ia FRBs can only be triggered at fairly low redshifts  $z \lesssim 0.7$ . A delay is required for type Ia FRBs with respect to type Ib FRBs (which track SFH). Quite different physical mechanisms are necessary for type Ia and Ib FRBs, respectively.

#### IV. DISCRIMINATING PROPERTIES

After the subclassification of type I FRBs, we would like to see their discriminating physical properties. It is worth noting that the only consideration in the previous section is whether one subclass of type I FRBs tracks SFH while the other subclass does not, namely we completely have not taken their physical

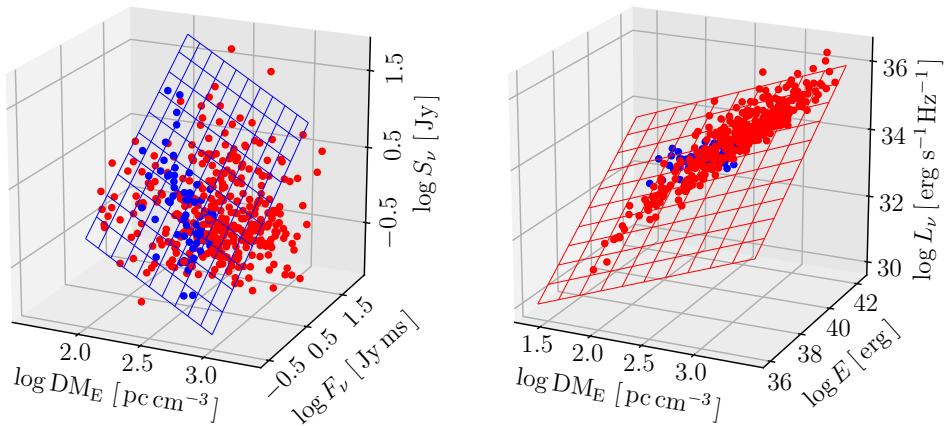


FIG. 9: Left panel: The 3-D empirical correlation (blue meshed plane) between fluence  $F_\nu$ , flux  $S_\nu$  and  $DM_E$  given in Eq. (16) for 65 type Ia FRBs (blue points), but no such correlation for 365 type Ib FRBs (red points). Right panel: The 3-D empirical correlation (red meshed plane) between spectral luminosity  $L_\nu$ , isotropic energy  $E$  and  $DM_E$  given in Eq. (27) for 365 type Ib FRBs (red points). The ones for 65 type Ia FRBs (blue points) and 430 type I FRBs (all points) are given in Eqs. (26) and (28), respectively. See Sec. IV for details.

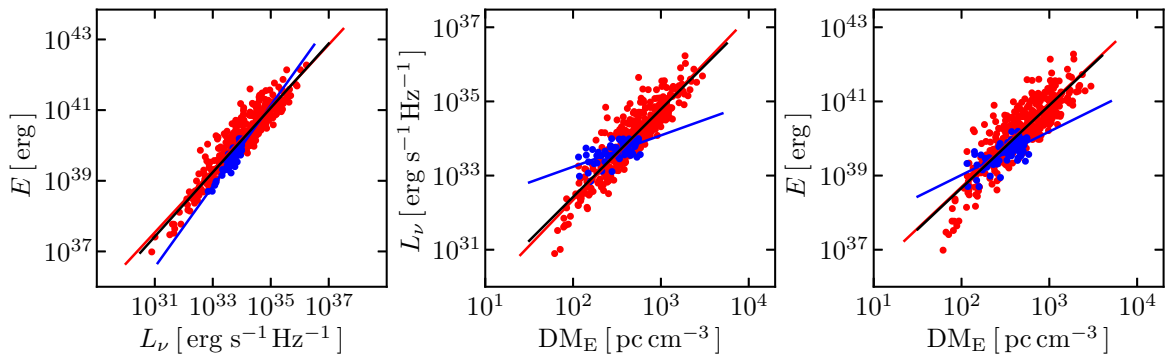


FIG. 10: The empirical correlations (blue/red/black lines) between spectral luminosity  $L_\nu$ , isotropic energy  $E$  and  $DM_E$  for 65 type Ia FRBs (blue points), 365 type Ib FRBs (red points), and 430 type I FRBs (all points), respectively. See Sec. IV for details.

properties into account when we made this subclassification. We identified type Ia and Ib FRBs only in the light of SFH. Logically, if they do come from different physical mechanisms, their physical properties might be also different in some aspects.

In Fig. 1 and panel (d) of Fig. 3, by definition, type Ia and Ib FRBs are clearly separated in the  $\nu W - L_\nu$  phase plane. Type Ia FRBs have relatively high brightness temperatures  $T_B$  and low spectral luminosities  $L_\nu$ , as required by Eq. (12). It is worth noting that we do not take transient duration  $\nu W$  into account when the physical conditions in Eq. (12) are determined. However, an upper boundary in  $\nu W$  naturally emerges for type Ia FRBs, namely  $\nu W \lesssim 2 \times 10^{-3}$  GHz s, which is determined by the right vertex of region (8) in Fig. 1 and panel (d) of Fig. 3. So, type Ia FRBs have also relatively short transient durations  $\nu W$ . Type Ib FRBs are the rest outside region (8). These two subclasses are clearly separated in this 2-D phase plane. Although they overlap each other in the  $DM_E - \log E$  plane, we find that type Ia and Ib FRBs are located in distinct regions if the third dimension  $\log T_B$  or  $\log \nu W$  is added, as shown in Fig. 7. Their separation in 3-D spaces also hints different physical mechanisms.

We try to find some empirical correlations for type Ia and Ib FRBs through trial and error. At first, we present the empirical correlations between fluence  $F_\nu$ , flux  $S_\nu$  and  $DM_E$ . In Fig. 8, we show the 2-D plots for these empirical correlations. Since our main purpose is to find the discriminating physical properties for type Ia and Ib FRBs, it is enough to fit the data without error bars (and we will take errors into account in the future works). This can be done by using `sklearn.linear_model.LinearRegression` in

Python [76]. The score (coefficient of determination) is given by  $R^2 \equiv 1 - \sum_k (y_k - \hat{y}_k)^2 / \sum_k (y_k - \bar{y})^2$ , where  $y_k$ ,  $\hat{y}_k$  and  $\bar{y}$  are the observed values, regressed values and mean of observed values [31, 76], respectively. The higher  $R$  indicates the better fit, and  $R = 1$  at best. As shown in Fig. 8, we find tight 2-D empirical correlations for 65 type Ia FRBs, namely

$$\log F_\nu = 0.7709 \log S_\nu + 0.3150, \quad \text{with } R = 0.9119, \quad (13)$$

$$\log \text{DM}_E = -0.3987 \log S_\nu + 2.5402, \quad \text{with } R = 0.8626, \quad (14)$$

$$\log F_\nu = -1.2873 \log \text{DM}_E + 3.6139, \quad \text{with } R = 0.7038. \quad (15)$$

On the contrary, there are no such correlations for 365 type Ib FRBs (since the corresponding  $R^2 < 0$ ), as expected by eyes. Putting Eqs. (13)–(15) together, it is anticipated that there is a tight 3-D empirical correlation between fluence  $F_\nu$ , flux  $S_\nu$  and  $\text{DM}_E$  for 65 type Ia FRBs. Fitting to the data, we find

$$\log S_\nu = -0.9468 \log \text{DM}_E + 0.7143 \log F_\nu + 2.1880, \quad \text{with } R = 0.9634, \quad (16)$$

which is a 2-D plane in the 3-D plot as shown in left panel of Fig. 9. Noting that its  $R$  is much higher than the ones of 2-D empirical correlations given in Eqs. (13)–(15), we recommend preferably using the tight 3-D empirical correlation given in Eq. (16). No such 3-D correlation for 365 type Ib FRBs.

On the other hand, we also find some empirical correlations between spectral luminosity  $L_\nu$ , isotropic energy  $E$  and  $\text{DM}_E$ . As shown by the blue lines in Fig. 10, we find the 2-D empirical correlations for 65 type Ia FRBs, namely

$$\log E = 1.1446 \log L_\nu + 1.0720, \quad \text{with } R = 0.9081, \quad (17)$$

$$\log L_\nu = 0.8470 \log \text{DM}_E + 31.5430, \quad \text{with } R = 0.6112, \quad (18)$$

$$\log E = 1.1698 \log \text{DM}_E + 36.6770, \quad \text{with } R = 0.6697. \quad (19)$$

There are similar 2-D empirical correlations for 365 type Ib FRBs as shown by the red lines in Fig. 10, but with quite different slopes and intercepts, namely

$$\log E = 0.8862 \log L_\nu + 10.0664, \quad \text{with } R = 0.9285, \quad (20)$$

$$\log L_\nu = 2.4707 \log \text{DM}_E + 27.3976, \quad \text{with } R = 0.9065, \quad (21)$$

$$\log E = 2.2345 \log \text{DM}_E + 34.2238, \quad \text{with } R = 0.8590. \quad (22)$$

Obviously, these fits are much better than the ones for 65 type Ia FRBs, since they have much higher  $R$ . If we instead consider all 430 type I FRBs as a whole, these 2-D empirical correlations become

$$\log E = 0.9106 \log L_\nu + 9.1906, \quad \text{with } R = 0.9249, \quad (23)$$

$$\log L_\nu = 2.3656 \log \text{DM}_E + 27.6917, \quad \text{with } R = 0.8952, \quad (24)$$

$$\log E = 2.2309 \log \text{DM}_E + 34.2027, \quad \text{with } R = 0.8575, \quad (25)$$

as shown by the black lines in Fig. 10. Obviously, they are very close to the ones for 365 type Ib FRBs. It is not surprising since 365 type Ib FRBs dominate the whole type I sample. In the light of the 2-D empirical correlations in Eqs. (17)–(25), it is anticipated that there is a tight 3-D empirical correlation between spectral luminosity  $L_\nu$ , isotropic energy  $E$  and  $\text{DM}_E$ . Fitting to the data, we find

$$\text{Type Ia: } \log L_\nu = 0.0079 \log \text{DM}_E + 0.7174 \log E + 5.2316, \quad \text{with } R = 0.9081, \quad (26)$$

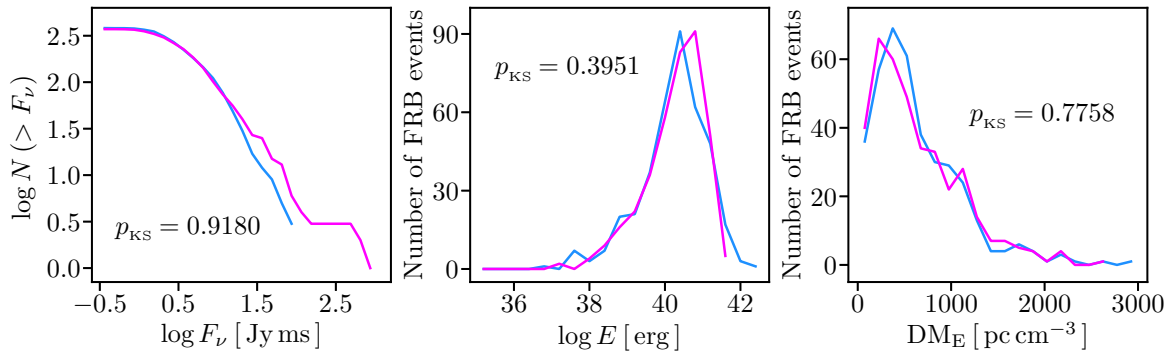
$$\text{Type Ib: } \log L_\nu = 1.1330 \log \text{DM}_E + 0.5986 \log E + 6.9098, \quad \text{with } R = 0.9525, \quad (27)$$

$$\text{Type I: } \log L_\nu = 1.0196 \log \text{DM}_E + 0.6033 \log E + 7.0561, \quad \text{with } R = 0.9460, \quad (28)$$

for 65 type Ia, 365 type Ib and all 430 type I FRBs, respectively. They are much better than the ones of 2-D empirical correlations in Eqs. (17)–(25), since they have much higher  $R$ . We recommend preferably using the tight 3-D empirical correlations given in Eqs. (26)–(28). In right panel of Fig. 9, we present the

$\log F_{\nu, \text{th}}^{\text{max}}$	$p_{\text{KS}}$ for $\log F_{\nu}$	$p_{\text{KS}}$ for $\log E$	$p_{\text{KS}}$ for $\text{DM}_{\text{E}}$
<b>0.95</b>	<b>0.9180</b>	<b>0.3951</b>	<b>0.7758</b>
0.96	0.8801	0.3928	0.7769
0.97	0.8504	0.3911	0.7120
0.99	0.7631	0.3868	0.6610
1.0	0.7036	0.3841	0.6185

TABLE III: The same as in Table I, but for 365 type Ib FRBs + 17 repeaters.

FIG. 11: The same as in Fig. 5, but for  $\log F_{\nu, \text{th}}^{\text{max}} = 0.95$  and 365 type Ib FRBs + 17 repeaters.

2-D plane corresponding to Eq. (27) in the 3-D plot. Although they have similar empirical correlations, type Ia and Ib FRBs are still distinguishable, due to their quite different slopes and intercepts.

So far, we show that type Ia and Ib FRBs have some discriminating physical properties. They can be clearly separated in the  $\nu W - L_{\nu}$  phase plane and some 3-D spaces. We find some tight empirical correlations for them, which can also be used to distinguish between type Ia and Ib FRBs. These results hint that they do come from different physical mechanisms.

## V. REPEATING FRBS

Let us turn to repeating (type II) FRBs. It is reasonable to also consider a similar subclassification of type II FRBs. As mentioned in Sec. II, there are only 17 repeaters after the robust cut, which are too few to form a good enough sample in statistics. But this does not prevent us from some exploratory studies.

The first question is whether there are subclasses of repeating (type II) FRBs? The answer is a clear yes. In the recent observations, some extragalactic repeaters were located in the star-forming environments, as mentioned in Sec. I. The Galactic repeater FRB 200428 has been firmly associated with the young magnetar SGR 1935+2154. On the other hand, the well-known repeating FRB 20200120E in a globular cluster is clearly associated with old stellar populations. These observations strongly suggest a similar subclassification of repeating (type II) FRBs: type IIa FRBs (e.g. FRB 20200120E) are associated with old stellar populations and hence do not track SFH, while type IIb FRBs (e.g. FRB 180916.J0158+65, FRB 121102, FRB 20190520B, FRB 20181030A, FRB 200428) are associated with young stellar populations and hence track SFH. Different physical mechanisms are required by type IIa and IIb FRBs.

The second question is whether there are two subclasses in the 17 repeaters of the first CHIME/FRB catalog? The answer might be not. It is reasonable to speculate that they are all type IIb FRBs, because (a) the known type IIa repeater associated with old stellar populations (i.e. FRB 20200120E) is not in the first CHIME/FRB catalog. (b) at least 16 of these 17 repeaters are clearly outside region (8) in the  $\nu W - L_{\nu}$  phase plane as shown in Fig. 1, while the only one just at the right vertex of region (8) can also

be excluded due to the uncertainty of the exact boundaries of region (8). (c) at least two of the known type IIb repeaters associated with young stellar populations (i.e. FRB 20121102A and FRB 20180916B (FRB 180916.J0158+65)) are in the first CHIME/FRB catalog, namely they are 2 of the 17 repeaters under discussion. (d) if these 17 repeaters are all type IIb FRBs, we could check this speculation by combining them with 365 type Ib FRBs and see whether these 382 FRBs track SFH (n.b. 17 repeaters are too few to do this alone since they cannot form a good enough sample in statistics). This can be tested by using the method mentioned in Sec. III B, and we present the results in Table III and Fig. 11. Clearly, these 382 FRBs can be fully consistent with SFH since three p-values  $p_{\text{KS}} > 0.39$  simultaneously for some suitable  $\log F_{\nu, \text{th}}^{\text{max}}$ . So, the possibility that these 17 repeaters are all type IIb FRBs (associated with young stellar populations and hence track SFH) cannot be excluded by now.

The third question is that could we speculate the physical criteria for the subclassification of type II FRBs? Let us try. It is natural to also subclassify type II FRBs in the  $\nu W - L_\nu$  phase plane, and the conservative physical criteria might be similar to the ones of type I FRBs, namely they might also be the dividing lines of  $L_\nu$  and  $T_B$  (and  $\nu W$ ). But it is reasonable that the dividing lines of  $L_\nu$  and  $T_B$  (and  $\nu W$ ) might be quite different from the ones of type I FRBs (namely  $L_{\nu, \text{crit}} = 10^{34}$  erg/s/Hz and  $T_{B, \text{crit}} = 2 \times 10^{35}$  K). For instance, a much lower  $T_{B, \text{crit}} = 10^{33}$  K was proposed for FRB 20121102A in [31], although their main purpose is somewhat different from ours. Here, we would like to make a bold but not too bold speculation. We strongly refer to Fig. 3 of [48] or Fig. 7 of [7], where the known repeater associated with old stellar populations (type IIa), i.e. FRB 20200120E, is plotted in the  $\nu W - L_\nu$  phase plane, together with the known repeaters associated with young stellar populations (type IIb), i.e. FRB 20180916B (FRB 180916.J0158+65), FRB 20121102A, FRB 20190711A, and the Galactic FRB 200428 (SGR 1935+2154). Thus, Fig. 3 of [48] or Fig. 7 of [7] are ideal test ground for the subclassification of type II FRBs. Similar to region (8) defined by Eq. (12) for type I FRBs, we speculate that the possible physical criteria for the subclassification of type II FRBs might be given by

$$\text{Type IIa : } L_\nu \lesssim 10^{29} \text{ erg/s/Hz} \quad \& \quad T_B \gtrsim 10^{30} \text{ K}, \quad (29)$$

$$\text{Type IIb : } \text{otherwise}. \quad (30)$$

Note that they are roughly estimated by eyes from Fig. 3 of [48] or Fig. 7 of [7], and hence they are not the exact ones. In this way, FRB 20200120E, the known type IIa repeater associated with old stellar populations, could be roughly separated from the known type IIb repeaters associated with young stellar populations mentioned above. If these physical criteria for the subclassification of type II FRBs given by Eqs. (29) and (30) are roughly correct, it is easy to see from Fig. 1 that the 17 CHIME repeaters are all type IIb FRBs, coincident with our discussions about the second question.

Although the number of repeaters under consideration is too few to go further, we have tried our best to subclassify the repeaters into type IIa and IIb FRBs, with good enough reasonings based on the observational facts. We stress that they are highly speculative. Since the data of repeaters will be rapidly accumulated in the future, we hope this subclassification of type II FRBs could be refined.

## VI. CONCLUDING REMARKS

Although FRBs have been an active field in astronomy and cosmology, their origin is still unknown to date. One of the interesting topics is the classification of FRBs, which is closely related to the origin of FRBs. Different physical mechanisms are required by different classes of FRBs. In the literature, they usually could be classified into non-repeating and repeating FRBs. Well motivated by the observations, here we are interested in the possible subclassification of FRBs. By using the first CHIME/FRB catalog, we propose to subclassify non-repeating (type I) FRBs into type Ia and Ib FRBs. The distribution of type Ia FRBs is delayed with respect to SFH, and hence they are probably associated with old stellar populations, while the distribution of type Ib FRBs tracks SFH, and hence they are probably associated with young stellar populations. Accordingly, the physical criteria for this subclassification of type I FRBs have been clearly determined. We find that there are some tight empirical correlations for type Ia FRBs but not for type Ib FRBs, and vice versa. These make them different in physical properties. Similarly, we suggest that repeating (type II) FRBs could also be subclassified into type IIa and IIb FRBs. This subclassification of FRBs might help us to reveal quite different physical mechanisms behind them, and improve their applications in astronomy and cosmology.

<b>FRBs</b>	<b>Class (a) :</b> associated with old stellar populations	<b>Class (b) :</b> associated with young stellar populations
<b>Type I :</b> Non-repeating	<b>Type Ia :</b> Non-repeating FRBs associated with old stellar populations and hence delayed with respect to SFH	<b>Type Ib :</b> Non-repeating FRBs associated with young stellar populations and hence track SFH
<b>Type II :</b> Repeating	<b>Type IIa :</b> Repeating FRBs associated with old stellar populations and hence delayed with respect to SFH	<b>Type IIb :</b> Repeating FRBs associated with young stellar populations and hence track SFH

TABLE IV: A brief summary of the universal subclassification scheme of FRBs.

In history, the subclassifications have made many important progresses in various fields. For example, the subclassification of supernovae is well known, as mentioned in Sec. I. The famous subclass of type Ia supernovae was identified in this way. Only they can be used as standard candles, which led to the great discovery of cosmic acceleration (and Nobel prize in physics 2011). This highlights the importance of the subclassifications. It might happen again in the field of FRBs. For instance, FRBs can be used to study cosmology, but the constraints on the cosmological parameters are usually loose (see e.g. [52–58]). If one of the subclasses of FRBs could be used as standard candles, rulers, or sirens (say, by the help of some unknown empirical correlations for this subclass of FRBs), we might remarkably improve the cosmological constraints in the future. Let us keep an open mind to this possibility.

In this work, we have identified 65 type Ia FRBs in the first CHIME/FRB catalog. They have relatively high brightness temperatures  $T_B$  and low spectral luminosities  $L_\nu$ , as required by Eq. (12). As shown in right panel of Fig. 4, type Ia FRBs can only be triggered at fairly low redshifts  $z \lesssim 0.7$ . A delay is required for type Ia FRBs with respect to type Ib FRBs (which track SFH). They are probably associated with old stellar populations. On the other hand, as mentioned at the beginning of Sec. IV, an upper boundary in  $\nu W$  naturally emerges for type Ia FRBs, namely  $\nu W \lesssim 2 \times 10^{-3}$  GHz s. So, type Ia FRBs have also relatively short transient durations  $\nu W$ . These properties might help us to reveal the physical mechanism for type Ia FRBs. For instance, the compact binary merger model in a rapid process might be one of the candidates. Gravitational waves (GWs) are usually expected in such a merger. Thus, we might witness type Ia FRBs as electromagnetic counterparts of GW events in the future. This might be a good chance to study gravity, cosmology and IGM.

As found in [49, 51], all FRBs in the first CHIME/FRB catalog as a whole do not track SFH. In this work, we have identified the main cause, namely 65 type Ia FRBs. If they are removed, the rest (mainly type Ib FRBs) do track SFH. In the future, numerous type I FRBs could be well located in their host galaxies, and hence they could be easily subclassified: the ones associated with old/young stellar populations are type Ia/Ib FRBs, respectively. So, one might only use type Ib FRBs to study cosmology and IGM. Thus, it is justified that today one can generate the mock sample of type Ib FRBs by simply assuming a redshift distribution tracking SFH, and use these mock type Ib FRBs to study cosmology and IGM. In this way, one might avoid to consider the complicated redshift distribution models, and hence the simulations could be significantly simplified.

Currently, many of well located FRBs are repeaters [18], thanks to their repeating behaviors. So, it is reasonable to expect that there will be many observational data for repeating (type II) FRBs well located in their host galaxies in the near future, and hence they could be easily subclassified: the ones associated with old/young stellar populations are type IIa/IIb FRBs, respectively. At that time, the physical criteria (in terms of e.g.  $L_\nu$ ,  $T_B$ ,  $\nu W$ ) for the subclassification of type II FRBs could be clearly determined. In turn, they could be used to subclassify the repeaters without well located host galaxies. This virtuous cycle will benefit the studies on repeating (type II) FRBs.

In Table IV, we present a brief summary of the universal subclassification scheme of FRBs. As in the literature, type I/II FRBs are non-repeating/repeating, respectively. Class (a)/(b) FRBs are associated with old/young stellar populations, respectively. Their combinations result in four subclasses: Ia, Ib, IIa, IIb,

I**b**, as shown in Table IV. The physical criteria for this subclassification given in Eqs. (12) and (29) are inferred by using the first CHIME/FRB catalog and Fig. 3 of [48] or Fig. 7 of [7], respectively. We stress that the physical criteria in Eqs. (12) and (29) might be changed for the larger and better FRB datasets in the future, but the universal subclassification scheme given in Table IV will always hold. Different physical mechanisms for FRBs are required by these subclasses. Note that the key improvement of the universal subclassification scheme given in Table IV is that it works even for a single FRB. A sample of FRBs is needed to see whether their distribution tracks SFH, while one cannot determine whether a single FRB tracks SFH or not. But even for a single FRB, its host galaxy and local environment can be precisely determined. If this FRB has been localized in a star-forming environment, it is a class (b) FRB. Otherwise, it is a class (a) FRB. Combining with whether it repeats, we can then determine its subclass to be one of Ia, Ib, IIa, IIb. In this way, no other criteria are needed (on the other hand, for a single FRB without identified host galaxy, we could instead subclassify it by using the physical criteria given in Eq. (12) or Eq. (29)).

It is of interest to speculate the possible progenitor theories for these four subclasses of FRBs. We refer to [16] for the up-to-date FRB theory catalogue. In general, since class (a) FRBs are associated with old stellar populations and hence delayed with respect to SFH, their progenitors might be formed via the compact binary merger which needs to undergo a long inspiral phase before the final coalescence, or the accretion-induced collapse of a white dwarf (WD) which also needs a long time to accrete before the final collapse. On the other hand, since class (b) FRBs are associated with young stellar populations and hence track SFH, their progenitors might be formed directly via the collapse of a massive star. Therefore, we speculate that type Ia FRB comes from the merger of neutron star (NS) – black hole (BH) binary or NS-NS binary (see Sec. 4.1 of [16]), and the final remnant of this merger is a black hole so that the resulted FRB is one-off. The progenitor of type IIa FRB might be the magnetar formed via the merger of WD-WD binary or the accretion-induced collapse of WD (see e.g. [47, 78]), while the magnetars similar to the well-known SGR 1935+2154 are the leading progenitors for the repeating FRBs. Similarly, the progenitor of type IIb FRB might be the young magnetar formed directly via the collapse of a massive star. The progenitor of type Ib FRB might be the supramassive NS formed via the collapse of a massive star, and it quickly collapses into a black hole or a quark star to produce a one-off FRB (see Sec. 4.2 of [16]). Of course, the above speculations are proposed just for examples. The other novel progenitor theories for these four subclasses of FRBs are all desirable.

We would like to briefly discuss the possible systematic errors. In generating the mock FRBs, the main systematic errors come from  $DM_{\text{IGM}}$ . In principle,  $DM_{\text{IGM}}$  should deviate from the mean given in Eq. (3) if the plasma density fluctuations are taken into account [83–85]. In the literature, the typical error in  $DM_{\text{IGM}}$  is  $\sigma_{\text{IGM}} \sim 100 \text{ pc cm}^{-3}$  [51–58, 83–85]. However, we stress that it is not a serious problem in the present work, because we are simulating a very large sample of mock FRBs ( $N_{\text{sim}} = 4,000,000$ ) and hence  $DM_{\text{IGM}}$  should heavily concentrate on the mean given in Eq. (3) [49]. Similarly, if we take the error of  $DM_{\text{host}}$  into account, it is also not a serious problem when we generate  $DM_{\text{E}}$  for a very large sample of mock FRBs ( $N_{\text{sim}} = 4,000,000$ ) [49]. On the other hand, our main goal is to subclassify FRBs, while the physical criteria given in Eq. (12) or Eq. (29) are very rough in fact. Some uncertainties in the boundaries of e.g. region (8) in the  $\nu W - L_{\nu}$  phase plane (see Fig. 1) only affect a few observed FRBs, and hence cannot significantly change the subclassification of FRBs. Of course, they should be carefully considered in the future works.

## ACKNOWLEDGEMENTS

We thank the anonymous referee for quite useful comments and suggestions, which helped us to improve this work. We are grateful to Da-Chun Qiang, Hua-Kai Deng, Shu-Ling Li, Shupeng Song, Jing-Yi Jia and Zi-Yu Hou for kind help and useful discussions. This work was supported in part by NSFC under Grants No. 11975046 and No. 11575022.

---

[1] <https://www.nature.com/collections/rswtktxcln>



- [2] D. R. Lorimer, *Nat. Astron.* **2**, 860 (2018) [arXiv:1811.00195].
- [3] E. F. Keane, *Nat. Astron.* **2**, 865 (2018) [arXiv:1811.00899].
- [4] M. Caleb, L. G. Spitler and B. W. Stappers, *Nat. Astron.* **2**, 839 (2018) [arXiv:1811.00360].
- [5] U. L. Pen, *Nat. Astron.* **2**, 842 (2018) [arXiv:1811.00605].
- [6] E. Petroff, J. W. T. Hessels and D. R. Lorimer, *Astron. Astrophys. Rev.* **27**, 4 (2019) [arXiv:1904.07947].
- [7] E. Petroff, J. W. T. Hessels and D. R. Lorimer, *Astron. Astrophys. Rev.* **30**, 2 (2022) [arXiv:2107.10113].
- [8] B. Zhang, *Nature* **587**, 45 (2020) [arXiv:2011.03500].
- [9] Y. Lyubarsky, *Universe* **7**, no.3, 56 (2021) [arXiv:2103.00470].
- [10] D. Xiao, F. Y. Wang and Z. G. Dai, *Sci. China Phys. Mech. Astron.* **64**, 249501 (2021) [arXiv:2101.04907].
- [11] M. Caleb and E. Keane, *Universe* **7**, no.11, 453 (2021).
- [12] L. Nicastro *et al.*, *Universe* **7**, no.3, 76 (2021) [arXiv:2103.07786].
- [13] J. M. Cordes and S. Chatterjee, *Ann. Rev. Astron. Astrophys.* **57**, 417 (2019) [arXiv:1906.05878].
- [14] M. Pilia, *Universe* **8**, 9 (2022) [arXiv:2203.04890].
- [15] S. Bhandari and C. Flynn, *Universe* **7**, no.4, 85 (2021).
- [16] E. Platts *et al.*, *Phys. Rept.* **821**, 1 (2019) [arXiv:1810.05836].  
The up-to-date FRB theory catalogue is available at <https://frbtheorycat.org>
- [17] E. Petroff *et al.*, *Publ. Astron. Soc. Austral.* **33**, e045 (2016) [arXiv:1601.03547].  
The up-to-date FRB Catalogue is available at <https://www.frbcat.org> and <https://www.wis-tns.org>
- [18] K. E. Heintz *et al.*, *Astrophys. J.* **903**, 152 (2020) [arXiv:2009.10747].  
The up-to-date compilation of all known FRB host galaxies is available at <https://frbhosts.org>
- [19] D. Palaniswamy, Y. Li and B. Zhang, *Astrophys. J. Lett.* **854**, no.1, L12 (2018) [arXiv:1703.09232].
- [20] S. Ai, H. Gao and B. Zhang, *Astrophys. J. Lett.* **906**, no.1, L5 (2021) [arXiv:2007.02400].
- [21] M. Caleb *et al.*, *Mon. Not. Roy. Astron. Soc.* **484**, 5500 (2019) [arXiv:1902.00272].
- [22] L. Connor *et al.*, *Mon. Not. Roy. Astron. Soc.* **497**, 3076 (2020) [arXiv:2003.11930].
- [23] M. Bagchi, *Astrophys. J. Lett.* **838**, no.2, L16 (2017) [arXiv:1702.08876].
- [24] S. Yamasaki, T. Totani and K. Kiuchi, *Publ. Astron. Soc. Jap.* **70**, no.3, 39 (2018) [arXiv:1710.02302].
- [25] J. I. Katz, arXiv:2203.03675 [astro-ph.HE].
- [26] J. I. Katz, *Mon. Not. Roy. Astron. Soc.* **513**, no.2, 1925 (2022) [arXiv:2201.02910].
- [27] T. Hashimoto *et al.*, *Mon. Not. Roy. Astron. Soc.* **498**, no.3, 3927 (2020) [arXiv:2008.09621].
- [28] S. Q. Zhong *et al.*, *Astrophys. J.* **926**, no.2, 206 (2022) [arXiv:2202.04422].
- [29] Z. Pleunis *et al.*, *Astrophys. J.* **923**, no.1, 1 (2021) [arXiv:2106.04356].
- [30] X. J. Li, X. F. Dong, Z. B. Zhang and D. Li, *Astrophys. J.* **923**, no.2, 230 (2021) [arXiv:2110.07227].
- [31] D. Xiao and Z. G. Dai, *Astron. Astrophys.* **657**, L7 (2022) [arXiv:2112.12301].
- [32] A. Chaikova, D. Kostunin and S. B. Popov, arXiv:2202.10076 [astro-ph.HE].
- [33] <https://en.wikipedia.org/wiki/Supernova>
- [34] B. Zhang *et al.*, *Astrophys. J. Lett.* **655**, L25 (2007) [astro-ph/0612238].
- [35] P. Kumar and B. Zhang, *Phys. Rept.* **561**, 1 (2014) [arXiv:1410.0679].
- [36] B. C. Andersen *et al.*, *Nature* **587**, no. 7832, 54 (2020) [arXiv:2005.10324].
- [37] C. D. Bochenek *et al.*, *Nature* **587**, no. 7832, 59 (2020) [arXiv:2005.10828].
- [38] L. Lin *et al.*, *Nature* **587**, no. 7832, 63 (2020) [arXiv:2005.11479].
- [39] C. K. Li *et al.*, *Nat. Astron.* **5**, 378 (2021) [arXiv:2005.11071].
- [40] S. P. Tendulkar *et al.*, *Astrophys. J. Lett.* **834**, no.2, L7 (2017) [arXiv:1701.01100].
- [41] B. Marcote *et al.*, *Nature* **577**, no.7789, 190 (2020) [arXiv:2001.02222].
- [42] C. H. Niu *et al.*, *Nature* **606**, no.7916, 873 (2022) [arXiv:2110.07418].
- [43] M. Bhardwaj *et al.*, *Astrophys. J. Lett.* **919**, no.2, L24 (2021) [arXiv:2108.12122].
- [44] L. Piro *et al.*, *Astron. Astrophys.* **656**, L15 (2021) [arXiv:2107.14339].
- [45] H. Xu *et al.*, arXiv:2111.11764 [astro-ph.HE].
- [46] M. Bhardwaj *et al.*, *Astrophys. J. Lett.* **910**, no.2, L18 (2021) [arXiv:2103.01295].
- [47] F. Kirsten *et al.*, *Nature* **602**, no.7898, 585 (2022) [arXiv:2105.11445].
- [48] K. Nimmo *et al.*, *Nat. Astron.* **6**, 393 (2022) [arXiv:2105.11446].
- [49] R. C. Zhang and B. Zhang, *Astrophys. J. Lett.* **924**, no.1, L14 (2022) [arXiv:2109.07558].
- [50] M. Amiri *et al.*, *Astrophys. J. Supp.* **257**, no.2, 59 (2021) [arXiv:2106.04352].  
The data for CHIME/FRB Catalog 1 in machine-readable format can be found via their public webpage at <https://www.chime-frb.ca/catalog>

- [51] D. C. Qiang, S. L. Li and H. Wei, JCAP **2201**, 040 (2022) [arXiv:2111.07476].
- [52] W. Deng and B. Zhang, Astrophys. J. **783**, L35 (2014) [arXiv:1401.0059].
- [53] Y. P. Yang and B. Zhang, Astrophys. J. **830**, no. 2, L31 (2016) [arXiv:1608.08154].
- [54] H. Gao, Z. Li and B. Zhang, Astrophys. J. **788**, 189 (2014) [arXiv:1402.2498].
- [55] B. Zhou, X. Li, T. Wang, Y. Z. Fan and D. M. Wei, Phys. Rev. D **89**, 107303 (2014) [arXiv:1401.2927].
- [56] D. C. Qiang, H. K. Deng and H. Wei, Class. Quant. Grav. **37**, 185022 (2020) [arXiv:1902.03580].
- [57] D. C. Qiang and H. Wei, JCAP **2004**, 023 (2020) [arXiv:2002.10189].
- [58] D. C. Qiang and H. Wei, Phys. Rev. D **103**, 083536 (2021) [arXiv:2102.00579].
- [59] K. Dolag *et al.*, Mon. Not. Roy. Astron. Soc. **451**, no.4, 4277 (2015) [arXiv:1412.4829].
- [60] J. X. Prochaska and Y. Zheng, Mon. Not. Roy. Astron. Soc. **485**, no.1, 648 (2019) [arXiv:1901.11051].
- [61] R. M. Shannon *et al.*, Nature **562**, no. 7727, 386 (2018).
- [62] J. X. Prochaska *et al.*, Science **366**, no. 6462, 231 (2019) [arXiv:1909.11681].
- [63] T. Hashimoto *et al.*, Mon. Not. Roy. Astron. Soc. **488**, no. 2, 1908 (2019) [arXiv:1907.11730].
- [64] J. M. Cordes and T. J. W. Lazio, astro-ph/0207156.
- [65] J. M. Cordes and T. J. W. Lazio, astro-ph/0301598.
- [66] <https://pypi.org/project/pygedm>
- [67] N. Aghanim *et al.*, Astron. Astrophys. **641**, A6 (2020) [arXiv:1807.06209].
- [68] B. Zhang, Astrophys. J. Lett. **867**, no.2, L21 (2018) [arXiv:1808.05277].
- [69] R. C. Zhang *et al.*, Mon. Not. Roy. Astron. Soc. **501**, 157 (2021) [arXiv:2011.06151].
- [70] M. Pietka, R. P. Fender and E. F. Keane, Mon. Not. Roy. Astron. Soc. **446**, 3687 (2015) [arXiv:1411.1067].
- [71] W. A. Majid *et al.*, Astrophys. J. Lett. **919**, no.1, L6 (2021) [arXiv:2105.10987].
- [72] [https://en.wikipedia.org/wiki/Kolmogorov-Smirnov\\_test](https://en.wikipedia.org/wiki/Kolmogorov-Smirnov_test)
- [73] <https://docs.scipy.org/doc/scipy/reference/generated/scipy.stats.kstest.html>
- [74] P. Chawla *et al.*, Astrophys. J. **927**, 35 (2022) [arXiv:2107.10858].
- [75] P. Madau and T. Fragos, Astrophys. J. **840**, no.1, 39 (2017) [arXiv:1606.07887].
- [76] [https://scikit-learn.org/stable/modules/generated/sklearn.linear\\_model.LinearRegression.html](https://scikit-learn.org/stable/modules/generated/sklearn.linear_model.LinearRegression.html)
- [77] K. Nimmo *et al.*, Astrophys. J. Lett. **927**, no.1, L3 (2022) [arXiv:2111.01600].
- [78] W. Lu, P. Beniamini and P. Kumar, Mon. Not. Roy. Astron. Soc. **510**, 1867 (2022) [arXiv:2107.04059].
- [79] R. Luo *et al.*, Mon. Not. Roy. Astron. Soc. **494**, 665 (2020) [arXiv:2003.04848].
- [80] P. Schechter, Astrophys. J. **203**, 297 (1976).
- [81] W. Lu and A. L. Piro, Astrophys. J. **883**, 40 (2019) [arXiv:1903.00014].
- [82] R. Luo *et al.*, Mon. Not. Roy. Astron. Soc. **481**, 2320 (2018) [arXiv:1808.09929].
- [83] M. McQuinn, Astrophys. J. Lett. **780**, L33 (2014) [arXiv:1309.4451].
- [84] K. Ioka, Astrophys. J. Lett. **598**, L79 (2003) [astro-ph/0309200].
- [85] M. Jaroszynski, Mon. Not. Roy. Astron. Soc. **484**, no.2, 1637 (2019) [arXiv:1812.11936].